2.N Nuclear Physics A259 (1976) 99—121; © North-Holland Publishing Co., Amsterdam

ON THE WKB APPROXIMATION TO DIRECT HEAVY-ION REACTIONS

S. LANDOWNE, C. H. DASSO, B. S. NILSSON, R. A. BROGLIA and Aa. WINTHER
The Niels Bohr Institute, University of Copenhagen, DK-2100 Copenhagen Ø, Denmark

Received 26 November 1975

Abstract: The WKB approximation is used to derive an expression for the usual DWBA amplitude which generalizes previous semiclassical approximations. Comparisons to cases of inelastic scattering and transfer reaction including recoil are given. The extension to the general coupled-channel problem is briefly discussed.

1. Introduction

The semiclassical description forms a convenient basis for a discussion of reactions between heavy nuclei. In this description the amplitudes on the different channels are solutions of time dependent first-order coupled equations which display the essential multistep character of the reaction processes and the subtle effects due to the non-orthogonality of the channel wave functions [1]). Also one obtains a unified description of grazing collisions, deep inelastic reactions and the formation of compound nuclei [2]).

The effects of interference between different classical trajectories leading to the same scattering angle can be included by keeping track of the phase shift along the trajectories. Similarly the effects of diffraction can be incorporated by allowing for complex trajectories [3])

A further improvement of the semiclassical description can be obtained by using an exact partial wave expansion of the full Schrödinger equation and solving the coupled radial equations in a WKB approximation. One is then led to a formulation in terms of coupled first-order equations in the relative distance which are very similar to the coupled equations in time mentioned above. This semiquantal description [4]), which includes diffraction and interference phenomena, still retains the simplicity of the semiclassical coupled equations and the simple mechanical picture they convey of the reaction.

So far, the semiquantal description has been especially explored for simple one and two step reactions utilizing an imaginary potential to describe the depopulation to channels that are not detected. The generalization of the semiquantal methods using WKB wave functions for complex potentials leads to a rather accurate description of elastic as well as inelastic scattering [3–7]).

In the present paper we shall explore the accuracy of this method in describing first-order transfer processes including recoil. In this context we introduce a convenient method for the calculation of the WKB partial wave matrix elements which are generalizations of the orbital integrals in the semiquantal description.

2. One-particle transfer in DWBA

We consider the reaction A(a, b)B where a = b+1 and B = A+1. Denoting the entrance channel by α and the exit channel by β, the transition amplitude in the distorted wave Born approximation is given by

$$T_{\beta\alpha} = \int \mathrm{d}\boldsymbol{r}_\alpha \int \mathrm{d}\boldsymbol{r}_{1\mathrm{b}}\, \chi_\beta^{(-)*}(\boldsymbol{k}_\beta, \boldsymbol{r}_\beta) f(\boldsymbol{r}_{1\mathrm{b}}, \boldsymbol{r}_{\mathrm{bA}}) \chi_\alpha^{(+)}(\boldsymbol{k}_\alpha, \boldsymbol{r}_\alpha). \tag{2.1}$$

The vectors $\boldsymbol{r}_\alpha = \boldsymbol{r}_{\mathrm{aA}}$ and $\boldsymbol{r}_\beta = \boldsymbol{r}_{\mathrm{bB}}$ are the relative c m. coordinates in the entrance and exit channels respectively, $\boldsymbol{r}_{1\mathrm{b}}$ is the coordinate of the transferred particle relative to the core b and $\boldsymbol{r}_{\mathrm{bA}}$ is the position of b with respect to A. The asymptotic momenta in the exit and entrance channels are given by $\hbar\boldsymbol{k}_\beta$ and $\hbar\boldsymbol{k}_\alpha$ respectively.

The two-dimensional form factor may be expanded as

$$f(\boldsymbol{r}_{1\mathrm{b}}, \boldsymbol{r}_{\mathrm{bA}}) = \sum_{JJ'\lambda} (I_\mathrm{A} M_\mathrm{A} JM | I_\mathrm{B} M_\mathrm{B})(I_\mathrm{b} M_\mathrm{b} J'M' | I_\mathrm{a} M_\mathrm{a})(\lambda\mu J'M' | JM) f_{\lambda\mu}(\boldsymbol{r}_{1\mathrm{b}}, \boldsymbol{r}_{\mathrm{bA}}), \tag{2.2}$$

where $I_t M_t$ indicate the spin and magnetic quantum numbers of the different nuclei involved in the reaction, λ is the transferred orbital angular momentum and $f_{\lambda\mu}$ is a tensor of rank λ, given in the post representation by

$$f_{\lambda\mu}(\boldsymbol{r}_{1\mathrm{b}}, \boldsymbol{r}_{\mathrm{bA}}) = \sum_{MM'} (\lambda\mu J'M' | JM) \frac{2\lambda+1}{2J'+1} \times \int \mathrm{d}\zeta_1\, \phi_{JM}^{\mathrm{B(A)}*}(\boldsymbol{r}_{1\mathrm{A}}, \zeta_1)[U_{1\mathrm{b}}(r_{1\mathrm{b}}) - \langle U_{1\mathrm{b}} \rangle] \phi_{J'M'}^{\mathrm{a(b)}}(\boldsymbol{r}_{1\mathrm{b}}, \zeta_1). \tag{2.3}$$

The single particle wave functions $\phi^{\mathrm{B(A)}}$ and $\phi^{\mathrm{a(b)}}$ describe the motion of the transferred particle around the core A in the exit channel and around the core b in entrance channel respectively, ζ_1 being the spin coordinate. The interaction in (2.3) is the difference between the single-particle potential $U_{1\mathrm{b}}$ binding the particle to the core b and its expectation value in the exit channel as defined in ref. [8]).

In order to evaluate (2 1) we expand the distorted waves in terms of partial waves as follows:

$$\chi^{(-)*}(\boldsymbol{k}, \boldsymbol{r}) = \chi^{(+)}(-\boldsymbol{k}, \boldsymbol{r}) = \frac{4\pi}{kr} \sum_{lm} i^{-l}\, \mathrm{e}^{\mathrm{i}(\sigma_l + \delta_l)} \chi_l(k, r) Y_{lm}(\hat{\boldsymbol{k}}) Y_{lm}^*(\hat{\boldsymbol{r}}). \tag{2.4}$$

We have divided the total phase shifts into a nuclear part δ_l and a Coulomb part σ_l given by

$$\sigma_l = \arg\Gamma(l+1+i\eta), \tag{2.5}$$

where $\eta = Z_1 Z_2 e^2/\hbar v$ is the Coulomb parameter. The radial wave functions are regular at the origin and have the asymptotic behaviour ($r \to \infty$)

$$\chi_l(k, r) = \sin(kr - \tfrac{1}{2}\pi - \eta \ln(2kr) + \sigma_l + \delta_l). \tag{2.6}$$

Note that the χ_l are real if the optical potential has no imaginary part.

Substituting (2.4) and (2.2) into (2.1) the evaluation of $T_{\beta\alpha}$ is reduced to the calculation of the matrix element

$$t_{\beta\alpha} = \int d\boldsymbol{r}_\alpha \int d\boldsymbol{r}_{1b} \frac{\chi_{l_\beta}(k_\beta, r_\beta)}{r_\beta} \frac{\chi_{L_\alpha}(k_\alpha, r_\alpha)}{r_\alpha} Y^*_{l_\beta m_\beta}(\hat{r}_\beta) f_{\lambda\mu}(\boldsymbol{r}_{1b}, \boldsymbol{r}_{bA}) Y_{l_\alpha m_\alpha}(\hat{r}_\alpha). \tag{2.7}$$

In order to exploit the localization of the form factor (2.3) one should measure the coordinate of the transferred particle from a point β on the line connecting the cores b and A which lies at the surface of nucleus b. The geometrical relation between this vector, $\boldsymbol{r}_{1\beta}$, and the various other vectors is shown in fig. 1. One finds, for instance,

$$\boldsymbol{r}_\beta = s_B \boldsymbol{r}_\alpha - t_\beta \boldsymbol{r}_{1\beta}, \tag{2.8}$$

where

$$s_B = m_a(m_B - \beta m_1)/m_B(m_b + \beta m_1), \tag{2.9}$$

$$t_\beta = m_1(m_a + m_A)/(m_b + \beta m_1)m_B \tag{2.10}$$

Using $\boldsymbol{r}_{1\beta}$ as an integration variable instead of $\boldsymbol{r}_{1b}$ gives rise to a Jacobian

$$J = (m_B/m_B - \beta m_1)^3. \tag{2.11}$$

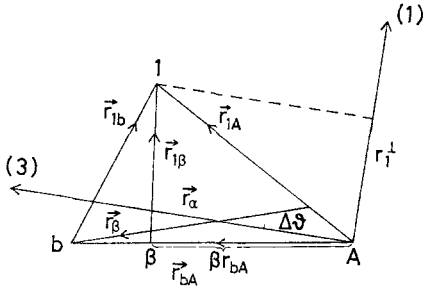

Fig 1 The geometrical relation between the various vectors in the DWBA matrix element. The point β is defined to lie on $\boldsymbol{r}_{bA}$ at a distance βr_{bA} from A

Next we introduce an intrinsic coordinate system with the 3-axis along $\boldsymbol{r}_\alpha$ and such that the transferred particle lies in the (1, 3) plane with a positive 1-component. We thus find

$$f_{\lambda\mu}(\boldsymbol{r}_{1b}, \boldsymbol{r}_{bA}) = \sum_{\mu'} D^\lambda_{\mu\mu'}(\varphi, \theta, \psi) f^{\text{intr}}_{\lambda\mu'}(r^{||}_{1\beta}, r_1^\perp, r_\alpha), \tag{2.12}$$

where the expression for $f^{\text{intr}}_{\lambda\mu}$ is formally the same as (2.3) except that the azimuthal angles in both single-particle wave functions are zero and the polar angles are measured

from the vector r_α. Thus $f^{\text{intr}}_{\lambda\mu}$ depends only on the shape of the triangle in fig. 1 as specified by the longitudinal component $(r_{1\beta})_3 = r^{\|}_{1\beta}$ and transverse component $(r_{1\beta})_1 = r^{\perp}_1$ of $r_{1\beta}$ and on the modulus of r_α. The Eulerian angles θ and φ are the polar coordinates of r_α while ψ specifies the last rotation bringing the (1, 3) plane into the plane of fig 1.

Similarly we find

$$Y^*_{l_\beta m_\beta}(\hat{r}_\beta) = \sum_{m_{\beta'}} D^{l_\beta *}_{m_\beta m_{\beta'}}(\varphi, \theta, \psi) Y^*_{l_\beta m_{\beta'}}(\Delta\theta, \pi), \tag{2.13}$$

where $\Delta\theta$ is the (small) angle between r_β and r_α, i.e.

$$\sin \Delta\theta = t_\beta r^{\perp}_1 / r_\beta . \tag{2.14}$$

Inserting (2.12) and (2.13) in (2.7) we can perform the integration over the angles φ, θ and ψ to find

$$t_{\beta\alpha} = \frac{4\pi}{2l_\beta+1} (\lambda\mu l_\alpha m_\alpha | l_\beta m_\beta) \sqrt{\frac{2l_\alpha+1}{4\pi}}\, I_{\beta\alpha}, \tag{2.15}$$

with

$$I_{\beta\alpha} = 2\pi \int_0^\infty r_\alpha^2 \mathrm{d}r_\alpha \int_{r_1{}^\perp > 0} r^{\perp}_1 \mathrm{d}r^{\perp}_1 \mathrm{d}r^{\|}_{1\beta} \frac{\chi_{l_\beta}(k_\beta, r_\beta)}{r_\beta} \frac{\chi_{l_\alpha}(k_\alpha, r_\alpha)}{r_\alpha} F_{\beta\alpha}(r^{\|}_{1\beta}, r^{\perp}_1, r_\alpha), \tag{2.16}$$

where

$$F_{\beta\alpha}(r^{\|}_{1\beta}, r^{\perp}_1, r_\alpha) = J \sum_{\mu'} (\lambda\mu' l_\alpha 0 | l_\beta \mu') Y_{l_\beta - \mu'}(\Delta\theta, 0) f^{\text{intr}}_{\lambda\mu'}(r^{\|}_{1\beta}, r^{\perp}_1, r_\alpha) \tag{2.17}$$

The length of r_β can be obtained in terms of r_α, $r^{\|}_{1\beta}$ and $r^{\perp}_1$ by eq. (2 8) The terms with $\mu' < 0$ can be obtained from the terms with $\mu' > 0$ by the symmetry relation

$$f^{\text{intr}}_{\lambda\mu'} = (-)^{\lambda+\pi+\mu'} f^{\text{intr}}_{\lambda-\mu'}, \tag{2.18}$$

where π is the total parity change in the reaction This leads to the selection rule $l_\alpha + l_\beta + \pi$ = even while the $\mu' = 0$ term has the selection rule $l_\alpha + l_\beta + \lambda$ = even.

In order to evaluate (2.16) numerically we perform a Taylor expansion of the exit channel wave function about the point $s_{\mathrm{B}} r_\alpha$; that is,

$$\chi_{l_\beta}(k_\beta, r_\beta) = \sum_\nu \frac{\chi^{(\nu)}_{l_\beta}(k_\beta, s_{\mathrm{B}} r_\alpha)}{\nu!} (r_\beta - s_{\mathrm{B}} r_\alpha)^\nu, \tag{2.19}$$

where the superscript (ν) denotes the *vth* derivative with respect to r_β We can then write the integral (2.16) in the form

$$I_{\beta\alpha} = \int_0^\infty \mathrm{d}r_\alpha \{ \sum_\nu \chi^{(\nu)}_{l_\beta}(k_\beta, s_{\mathrm{B}} r_\alpha) r^\nu_\alpha F^\nu_{\beta\alpha}(r_\alpha) \} \chi_{l_\alpha}(k_\alpha, r_\alpha), \tag{2.20}$$

where

$$F^\nu_{\beta\alpha}(r_\alpha) = \frac{2\pi}{\nu!} \int_{r_1{}^\perp > 0} r^{\perp}_1 \mathrm{d}r^{\perp}_1 \mathrm{d}r^{\|}_{1\beta} \frac{r_\alpha}{r_\beta} \left(\frac{r_\beta - s_{\mathrm{B}} r_\alpha}{r_\alpha} \right)^\nu F_{\beta\alpha}(r^{\|}_{1\beta}, r^{\perp}_1, r_\alpha) \tag{2.21}$$

For further details we refer to ref [8]).

3. The WKB approximation

3 1 WAVE FUNCTIONS

In calculating the matrix elements like (2.20) well below the Coulomb barrier in both entrance and exit channels, one can approximate the regular wave functions χ_l by the WKB solution

$$\tilde{\chi}_l(r) = \begin{cases} \sqrt{k/\hbar(r)}\,\sin\left(\int_{r_0}^{r} \hbar(r')\mathrm{d}r' + \tfrac{1}{4}\pi\right), & r > r_0 \qquad (3.1a) \\ \tfrac{1}{2}\sqrt{k/\kappa(r)}\,\exp\left(\int_{r_0}^{r} \kappa(r')\mathrm{d}r'\right), & r < r_0\,. \qquad (3.1b) \end{cases}$$

where the local wave number is given by

$$\hbar(r) = k\sqrt{1 - V_{\mathrm{eff}}(r)/E}, \qquad (3.2)$$

while

$$\kappa(r) = k\sqrt{V_{\mathrm{eff}}(r)/E - 1}. \qquad (3.3)$$

The asymptotic wave number k is related to the c.m. energy E by the relation $E = \hbar^2 k^2/2m$ where m is the reduced mass. The effective potential is

$$V_{\mathrm{eff}}(r) = \frac{\hbar^2(l+\frac{1}{2})^2}{2mr^2} + U(r) - iW(r), \qquad (3.4)$$

where $U - iW$ is the complex optical potential.

For real potentials there are usually three turning points r_0 satisfying the relation

$$\hbar(r_0) = 0. \qquad (3.5)$$

Well below the barrier only the real, outermost turning point is to be used in (3.1). When an absorptive potential iW is introduced this outermost turning point is shifted into the lower half of the complex r-plane, but the approximation (3.1) is still valid [4]) provided one defines the square roots in (3.2) and (3.3) to have positive imaginary and positive real parts respectively. The point on the real axis at which one should switch from the sine function to the exponential function is not clearly defined by (3 1). However for $r \approx \mathrm{Re}\, r_0$, of the two exponential terms in the sine function (3.1a), one coincides with (3.1b) while the other is exponentially small; actually smaller the further the turning point is away from the real axis.

One may utilize the above considerations on the WKB solutions for reactions with energies above the Coulomb barrier. In this case one also finds three turning points. Provided $W = 0$, one of them (the innermost) is real, while the other two are complex conjugate to each other and have a real part close to the radius of the Coulomb barrier By appropriately choosing the sign of the square root in (3.3) one can write three WKB solutions to the wave equation inserting each of these turning points into

(3.1). While for the innermost turning point (3.1) can be used directly for all values of r, the solutions associated with the complex turning points have purely incoming or outgoing waves inside the Coulomb barrier since κ is purely imaginary in this region. If the turning point in the lower half-plane is used in (3.1), an almost continuous WKB solution is obtained along the real axis by choosing $\mathrm{Im}\,\kappa < 0$, while for the other complex turning point an equivalent approximation is obtained choosing $\mathrm{Im}\,\kappa > 0$ Note that these two WKB solutions are complex conjugates (time reverses) of each other.

The solution associated with the real turning point has standing waves inside the Coulomb barrier, while the solutions corresponding to the turning points lying in the upper and lower half-plane have the boundary condition of outgoing and incoming waves respectively in this region. Because of the many reactions taking place inside the barrier the latter boundary condition corresponds to the true physical situation

In what follows we will use this solution associated with the lower turning point as the WKB approximation to the distorted waves of sect 2 for general potentials with an imaginary part W acting as a sink inside the nucleus†. In the surface region W is small compared to the real potential and we may consider the effect of the imaginary potential as a small perturbation. The complex turning point is then given, in terms of the turning point $\tilde{r}_0$ for $W = 0$, by the relation

$$r_0 = \tilde{r}_0 + \imath W(\tilde{r}_0) \Big/ \frac{\mathrm{d}V_{\mathrm{eff}}}{\mathrm{d}r}\bigg|_{\tilde{r}_0}. \tag{3.6}$$

It is seen from (3.6) that the turning point in the lower half-plane moves continuously into the outermost turning point as the energy is decreased from above to below the the Coulomb barrier. The turning point on the inside of the Coulomb barrier is similarly continuously connected with the turning point in the upper half-plane and never coalesces with the turning point on the outside of the barrier.

In subsect. 3.2 we show how to recast the DWBA matrix element in the WKB approximation into a path integral in the complex plane. For this purpose we need the WKB solution (3.1) to the wave equation in the entire complex plane as discussed in ref. [7]). We write this solution in the form

$$\tilde{\chi}_l(r) = \begin{cases} \frac{1}{2}[\psi_l^{\mathrm{in}}(r) + \psi_l^{\mathrm{out}}(r)] & \text{inside } \mathscr{D} \\ \frac{1}{2}\psi_l^{\mathrm{reg}}(r) & \text{outside } \mathscr{D}. \end{cases} \tag{3.7}$$

The domain $\mathscr{D}$ (see fig 2) is defined as the region between the Stokes lines S_2 and S_3 emerging from the outer turning point. The Stokes lines are formed by the points r satisfying the relation

$$\mathrm{Re}\int_{r_0}^{r} k(r')\mathrm{d}r' = 0. \tag{3.8}$$

† The WKB solution associated with the upper turning point, being the complex conjugate of this solution, corresponds to the situation where W acts as a source

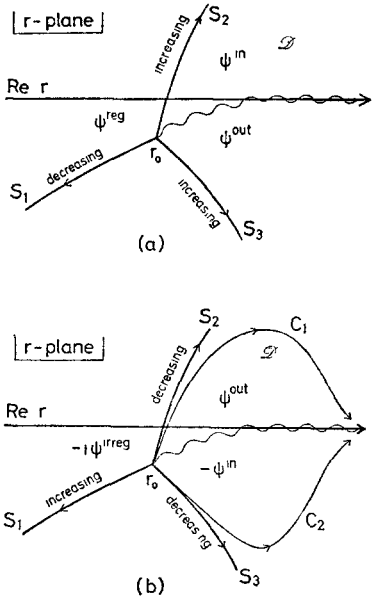

Fig 2 The analytic continuation of ψ^{in} [cf eq. (3 9)] On the first sheet (a), above the cut indicated by the wavy line, ψ^{in} represents an incoming wave for large values of r. As ψ^{in} is continued anticlockwise around r_0 it becomes exponentially increasing along Stokes line S_2, decreasing along Stokes line S_1 and increasing along Stokes line S_3. Below the cut in region $\mathscr{D}$ the continuation of ψ^{in} is the outgoing wave ψ^{out} given by (3.10) As the anticlockwise continuation proceeds through the cut the second sheet is entered. The behaviour under further continuation in the second sheet is shown in (b). The values of the function in the third and fourth Riemann sheets are obtained from those in the first and second sheets, respectively, by an overall change of sign The further continuation from the fourth sheet anticlockwise leads into the first sheet

There are three such lines emerging from r_0 which, close to r_0, are separated 120° from each other [9]).

The wave functions ψ^{in}, ψ^{out} and ψ^{reg} are defined by

$$\psi_l^{in}(r) = e^{\frac{1}{2}i\pi}\sqrt{\frac{k}{\hbar(r)}}\exp\left[-i\int_{r_0}^{r}\hbar(r')dr'\right], \tag{3.9}$$

$$\psi_l^{out}(r) = e^{-\frac{1}{2}i\pi}\sqrt{\frac{k}{\hbar(r)}}\exp\left[i\int_{r_0}^{r}\hbar(r')dr'\right], \tag{3 10}$$

$$\psi_l^{reg}(r) = \sqrt{\frac{k}{\kappa(r)}}\exp\left[\int_{r_0}^{r}\kappa(r')dr'\right], \tag{3 11}$$

where $0 \leqq \arg k(r) < \pi$ and $|\arg \kappa(r)| < \frac{1}{2}\pi$.

The functions (3 9) – (3.11) are defined on four Riemann sheets. Two of these sheets, joined along a cut in the region $\mathscr{D}$, are illustrated in fig 2. The analytic continuation of ψ^{in} anticlockwise above r_0 becomes identical to ψ^{reg} [cf. fig 2(a)] and the

further analytic continuation of this function below r_0 brings it into ψ^{out}. If the function ψ^{out} is further continued anticlockwise above r_0 it goes into the irregular solution† along S_1 and finally into $-\psi^{\text{in}}$ in the region $\mathscr{D}$ [cf fig. 2b]

3.2. MATRIX ELEMENTS

We now turn to the evaluation of the matrix element (2.16). The turning points corresponding to entrance and exit channels are illustrated in fig. 3 together with the associated Stokes lines. As a first step we deform the path of integration in (2.16) from the real axis to a path P that goes through the two turning points as indicated in fig. 3. The two integrals (from 0 to ∞) are equal insofar as the region between the two paths does not contain any singularity of the integrand.

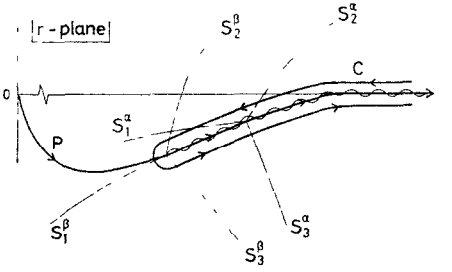

Fig. 3. Turning points and their associated Stokes lines for entrance and exit channels. The path P is used to evaluate the DWBA radial integral. The path C may be used to evaluate the WKB approximation to the radial integral The wavy line indicates cuts associated with the turning points.

The sequence in which the path P goes through the turning points r_0^α and r_0^β is such that it first encounters the point whose domain $\mathscr{D}$ contains the other turning point. This prescription is unique when the turning points are well separated and close to the real axis If the turning points are close together or far below the real axis the sequence is irrelevant for practical purposes.

Having deformed the path of integration to P, we now substitute the WKB approximations (3.7) for the entrance and exit channel wave functions in (2 16). Considering the exit channel, we use

$$r_\beta \approx s_B r_\alpha - t_\beta r_{1\beta}^{\|}, \tag{3.12}$$

in the argument of $\tilde{\chi}_{l_\beta}$ having neglected terms of the order $(t_\beta r_{1\beta}^{\|}/r_\beta)^2$ [cf. ref. [8])]. Thus we use

$$\tilde{\chi}_{l_\beta}(r_\beta) = \begin{cases} \tfrac{1}{2}[\psi_{l_\beta}^{\text{in}}(s_B r_\alpha)\exp[\imath K^{\|}(s_B r_\alpha) r_{1\beta}^{\|}] + \psi_{l_\beta}^{\text{out}}(s_B r_\alpha)\exp[-\imath K^{\|}(s_B r_\alpha) r_{1\beta}^{\|}]], & \text{inside } \mathscr{D} \\ \tfrac{1}{2}\psi_{l_\beta}^{\text{reg}}(s_B r_\alpha)\exp[\imath \bar{K}^{\|}(s_B r_\alpha) r_{1\beta}^{\|}], & \text{outside } \mathscr{D}, \end{cases} \tag{3.13}$$

† The function ψ^{irreg} is given by (3 11) with a minus sign in the exponent.

where, consistent within the WKB approximation, we have neglected the variation in $(k_\beta(r_\beta))^{-\frac{1}{2}}$ and $(\kappa_\beta(r_\beta))^{-\frac{1}{2}}$ as functions of $r_{1\beta}$. The quantity

$$K^{\|}(r) = t_\beta k_\beta(r), \tag{3.14a}$$

corresponds to the classical longitudinal component of the local momentum of the transferred particle while

$$\bar{K}^{\|}(r) = it_\beta \kappa_\beta(r). \tag{3.14b}$$

We also use in eq. (2.17) the expression

$$Y_{l_\beta - m}(\Delta\theta, 0) \approx \sqrt{\frac{2l_\beta+1}{4\pi}}\, J_m(K^\perp r_1^\perp), \tag{3.15}$$

where

$$K^\perp = t_\beta(l_\beta + \tfrac{1}{2})/s_B r_\alpha, \tag{3.16}$$

represents the classical perpendicular component of the local momentum of the transferred particle. The result (3.15) comes from the large l_β limit and from approximating $\sin\Delta\theta \approx \Delta\theta$ in (2.14) consistent with the approximation (3.12). Finally in (2.16) we set $1/r_\beta$ equal to $1/s_B r_\alpha$.

Under the above considerations the integral (2.16) is written as

$$\begin{aligned} I_{\beta\alpha} = \sum_{\mu'} (\lambda\mu' l_\alpha 0 | l_\beta \mu') \sqrt{\frac{2l_\beta+1}{4\pi}}\, \frac{1}{2} \Big\{ & \int_{r_0^\beta/s_B}^{\infty} \mathrm{d}r_\alpha \psi_{l_\beta}^{\mathrm{out}}(s_B r_\alpha) f_{\lambda\mu'}(-K^{\|}, K^\perp, r_\sigma) \tilde{\chi}_{l_\alpha}(r_\alpha) \\ & + \int_{r_0^\beta/s_B}^{\infty} \mathrm{d}r_\alpha \psi_{l_\beta}^{\mathrm{in}}(s_B r_\alpha) f_{\lambda\mu'}(K^{\|}, K^\perp, r_\alpha) \tilde{\chi}_{l_\alpha}(r_\alpha) \\ & + \int_0^{r_0^\beta/s_B} \mathrm{d}r_\alpha \psi_{l_\beta}^{\mathrm{reg}}(s_B r_\alpha) f_{\lambda\mu'}(\bar{K}^{\|}, K^\perp, r_\alpha) \tilde{\chi}_{l_\alpha}(r_\alpha) \Big\}, \end{aligned} \tag{3.17}$$

where

$$\begin{aligned} f_{\lambda\mu'}(K^{\|}, K^\perp, r_\alpha) = \frac{2\pi J}{s_B} \int_{r_1^\perp > 0} & r_1^\perp \mathrm{d}r_1^\perp \mathrm{d}r_{1\beta}^{\|}\, \mathrm{e}^{\mathrm{i}K^{\|}(s_B r_\alpha) r_{1\beta}^{\|}} \\ & \times J_{\mu'}(K^\perp(s_B r_\alpha) r_1^\perp) f_{\lambda\mu'}^{\mathrm{intr}}(r_{1\beta}^{\|}, r_1^\perp, r_\alpha). \end{aligned} \tag{3.18}$$

Outside the turning points, on the real axis, the form factor (3 18) is identical to the semiclassical form factor [1,8])

Next we insert the expression (3 7) for the radial wave function in the entrance channel Of the resulting seven terms we neglect

$$\int_0^{r_0^\beta/s_B} \mathrm{d}r_\alpha \psi_{l_\beta}^{\mathrm{reg}}(s_B r_\alpha) f_{\lambda\mu'}(\bar{K}^{\|}, K^\perp, r_\alpha) \psi_{l_\alpha}^{\mathrm{reg}}(r_\alpha), \tag{3.19}$$

as both wave functions are exponentially decreasing from the upper limit. In the same approximation we can neglect the integrals from r_0^α to ∞ containing the product $\psi_{l_\alpha}^{\mathrm{in}} \psi_{l_\beta}^{\mathrm{in}}$ since we can deform the path of integration to follow the Stokes line S_3^α down in the fourth quadrant, closing the path at infinity where the form factor vanishes.

Along this path, C_2, both functions are exponentially decreasing as indicated in fig. 2b. A similar argument applies to the term containing the product $\psi^{\text{out}}_{l_\beta}\psi^{\text{out}}_{l_\alpha}$ where the path C_1 following the Stokes line S_2^α in the first quadrant leads to exponentially decreasing functions.

The sum of the remaining four terms can be combined into a loop integral along C which circumvents both turning points (cf. fig 3) i e

$$I_{\beta\alpha} = \sum_{\mu'} (\lambda\mu' l_\alpha 0 | l_\beta \mu') \sqrt{\frac{2l_\beta+1}{4\pi}} \left(-\frac{1}{4}\right) \int_C \mathrm{d}r_\alpha \psi^{\text{out}}_{l_\beta}(s_B r_\alpha) f_{\lambda\mu'}(-K^{\|}, K^{\perp}, r_\alpha) \psi^{\text{in}}_{l_\alpha}(r_\alpha)$$

$$= \sum_{\mu'} (\lambda\mu' l_\alpha 0 | l_\beta \mu') \sqrt{\frac{2l_\beta+1}{4\pi}} \left(-\frac{1}{4}\right) \sqrt{k_\beta k_\alpha}$$

$$\times \int_C \mathrm{d}r_\alpha f_{\lambda\mu'}(-K^{\|}, K^{\perp}, r_\alpha) \frac{\exp\left(i\left[\int_{r_0^\beta}^{s_B r_\alpha} k_\beta(r')\mathrm{d}r' - \int_{r_0^\alpha}^{r_\alpha} k_\alpha(r')\mathrm{d}r'\right]\right)}{\sqrt{k_\beta(s_B r_\alpha)}\sqrt{k_\alpha(r_\alpha)}}. \tag{3.20}$$

This result was obtained utilizing the properties illustrated in fig. 2. From eq. (3.20) it is seen explicitly how the DWBA matrix elements are only sensitive to the form factors from the complex turning point in the lower half-plane and out along the real axis.

In the applications we shall use a series expansion of the form factor (3.18) in powers of the longitudinal momentum i.e.

$$f_{\lambda\mu'}(K^{\|}, K^{\perp}, r_\alpha) = \sum_\nu (\imath K^{\|}(s_B r_\alpha) r_\alpha)^\nu f_{\lambda\mu'}(\nu, K^{\perp}, r_\alpha), \tag{3.21}$$

which corresponds to the Taylor expansion (2.19).

For the case where the turning points are located in the opposite sequence of that shown in fig 3 the same expression (3.20) applies provided the loop C starts below the cut and circumvents the turning points clockwise

If the two turning points are close together one may use either contour with essentially the same result In this case one can expand the phase difference

$$\Delta\phi = \int_{r_0^\beta}^{s_B r_\alpha} \mathrm{d}r\, k_\beta(r) - \int_{r_0^\alpha}^{r_\alpha} \mathrm{d}r\, k_\alpha(r), \tag{3.22}$$

appearing in (3.20) to first order in the energy difference $E(\beta)-E(\alpha)$, the angular momentum difference $l_\beta - l_\alpha$, the difference in reduced mass $m_\beta - m_\alpha$ and the difference in optical potential One finds

$$\Delta\phi = \frac{1}{\hbar}(E(\beta)-E(\alpha))t - (l_\beta - l_\alpha)\phi(t) + \frac{1}{\hbar}\int_0^t [U_\alpha(r(t')) - U_\beta(r(t')) + \tfrac{1}{2}(m_\beta - m_\alpha)(v(t'))^2]\mathrm{d}t'$$

$$+ \frac{1}{\hbar}\left(\frac{m_B}{m_b+m_B} - \beta\right) m_1 \boldsymbol{r}(t)\cdot\boldsymbol{v}(t). \tag{3.23}$$

We have here introduced the average position vector $r(t)$ between the classical motion in entrance and exit channel and the corresponding velocity $v(t) = \dot{r}(t)$ The quantity $\phi(t)$ is the azimuthal angle in the plane of the average orbit measured from its symmetry axis The phase (3.23) is identical to the phase appearing in the semiclassical description of transfer reactions [1]). The quantal reaction matrix is thus in this limit identical to the semiclassical reaction amplitude [cf eq. (2 4) in ref. [4])], if we are below the barrier For reactions above the barrier the semiclassical approximation still applies if one lets the time t in the neighborhood of $t = 0$ become complex such that the corresponding r-value encircles the outermost complex turning point [6]).

4. Applications

In this section we illustrate the WKB results given in sect. 3 by calculating the angular distribution for elastic and inelastic scattering and transfer reactions in first order perturbation theory.

4 1. TURNING POINTS

In fig. 4 we show the turning points in the elastic channel for the case $^{18}O + ^{58}Ni$ at 60 MeV. The parameters of the optical potential used are given in table 1. They were obtained in ref. [10]) by fitting the corresponding elastic scattering data. The potential is typical in that it gives rise to a well defined barrier in the surface region and strong absorption in the interior. We also show turning points when the imaginary part of the potential is set equal to zero. Thus it can be seen that for partial wave $l =$ 30 the energy is just below the barrier in the effective potential and all lower partial

TABLE 1

Optical parameters used in the calculations

Reaction	V (MeV)	W (MeV)	r_0 (fm)	a (fm)
$^{58}Ni(^{18}O, ^{18}O')$	−90 1	42 9	1.220	0.50
$^{48}Ca(^{14}N, ^{13}C)$	−70 0	10.0	1 225	0 65

waves surmount their respective barriers. For $50 \leqq l \leqq 85$ the minimum of the inner potential "pocket" is greater than the c m energy. For $l > 85$ the effective potential no longer exhibits a pocket.

In fig 4 we show the turning points which were calculated solving the equation $k(r_0) = 0$ numerically. For the outermost turning points where the imaginary potential, as is typical for heavy ion reactions, is small compared to the total real potential, one can calculate r_0 utilizing the linear approximation (3.6). The accuracy of this approximation is shown in fig 8.

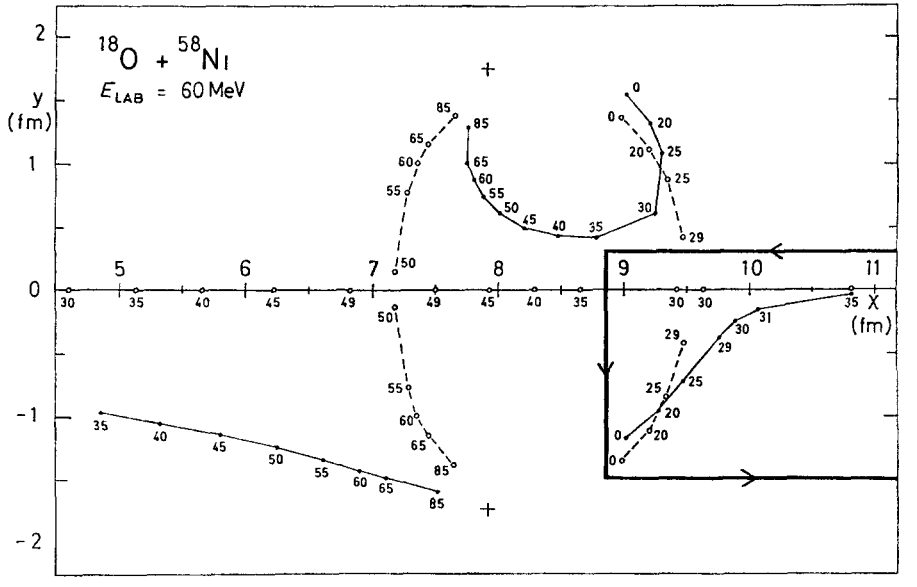

Fig 4 Complex turning points for $^{18}O+^{58}Ni$ at $E_{lab} = 60$ MeV calculated with the optical potential given in table 1. The open dots show the turning points when the imaginary potential is set to zero while the full dots are for the complex potential. The numbers give the angular momentum of various partial waves The solid line with arrows shows part of the integration path used in the WKB calculations. It returns to the real axis outside the range of interaction. The plus signs indicate positions of poles in the potential.

4.2. ELASTIC SCATTERING

The nuclear reflection coefficient η_l is defined in terms of the nuclear elastic phase shift δ_l as

$$\eta_l = e^{i2\delta_l} \tag{4.1}$$

The WKB approximation to the phase shift follows from the asymptotic form

$$\tilde{\chi}_l(r) = \sin(kr - \tfrac{1}{2}\pi l - \eta \ln(2kr) + \tilde{\sigma}_l + \tilde{\delta}_l), \tag{4.2}$$

of the WKB wave function (3.1). Here

$$\tilde{\sigma} = \eta \ln \sqrt{\eta^2 + (l+\tfrac{1}{2})^2} + (l+\tfrac{1}{2})\tan^{-1}(\eta/(l+\tfrac{1}{2})), \tag{4.3}$$

is the WKB Coulomb phase shift, which for large values of l has the same variation with l as (2 5)
The WKB nuclear phase shift can be written

$$\tilde{\delta}_l = \int_{r_0}^{R} k(r)\mathrm{d}r - \int_{r_0^C}^{R} k_C(r)\mathrm{d}r, \tag{4.4}$$

where $k_C(r)$ is the wave number in a pure Coulomb field, r_0^C being the corresponding turning point and R is a point on the real r-axis outside the range of the nuclear

potential. The second integral in (4.4) can be given in closed form while the first integral may be performed on any path from r_0 to R avoiding the singularities of $k(r)$. One may also use the expression

$$\int_{r_0}^{R} k(r)\mathrm{d}r = \frac{1}{2}\int_{C} k(r)\mathrm{d}r, \tag{4.5}$$

where C is a path of the type shown in fig. 3 beginning and ending at R circumventing the turning point r_0.

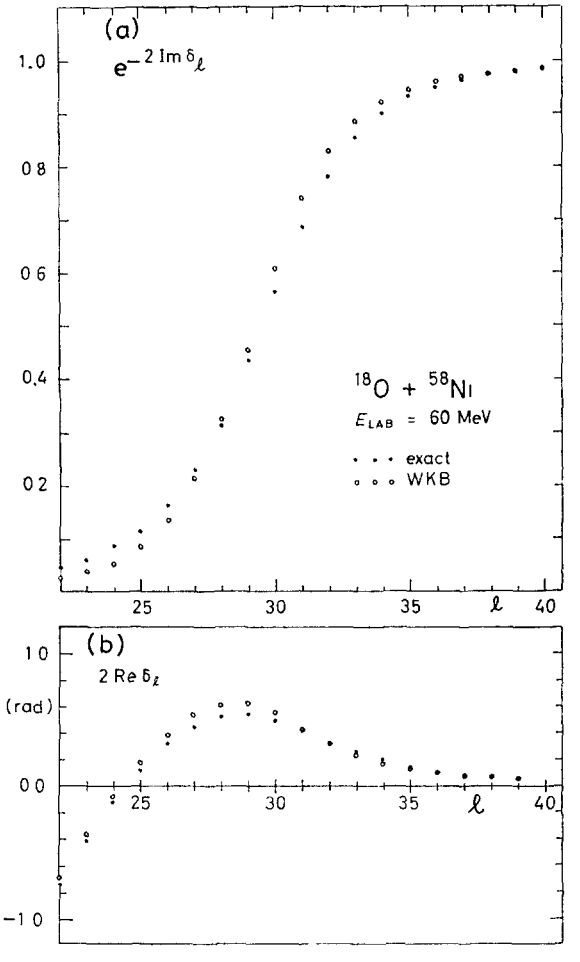

Fig 5. The magnitude (a) and phase (b) of the nuclear reflection coefficients for $^{18}O+^{58}Ni$ at E_{lab} = 60 MeV using the optical potential of table 1 The full dots are the results from integrating the Schrodinger equation numerically. The open dots are calculated in WKB approximation using the expression (4 4) and the outer turning points in the lower half-plane shown in fig. 4 (see also fig 8)

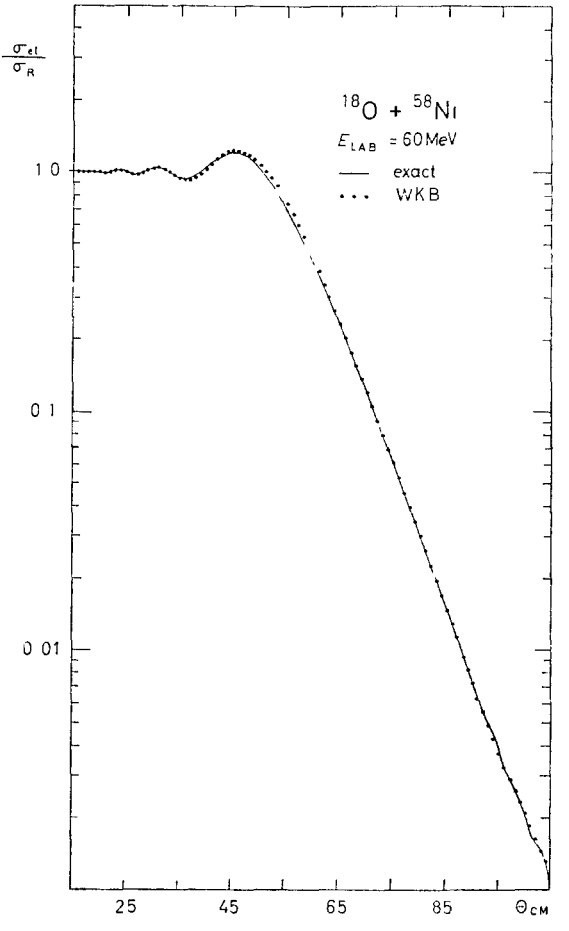

Fig 6 Elastic scattering angular distribution for $^{18}O+^{58}Ni$ at E_{lab} = 60 MeV calculated with the optical parameters in table 1 The reflection coefficients shown in fig. 5 were used in the calculations The full drawn curve is the result of a four parameter least-square fit to the elastic scattering data [10])

Having calculated the WKB phase shifts with (4.4), we display the corresponding reflection coefficients in fig. 5 in comparison with exact optical model calculations for the case of $^{18}O+^{58}Ni$ discussed above Similar results for other cases have been given in refs. [5, 6]) They show a major improvement over the corresponding results presented in ref. [4]) [cf *ibid.* case III, fig 4.1].

It is seen from the turning points in fig 4 that the phase shifts depend only on the tail of the optical potential. Since the imaginary potential is small in the surface region, the results shown in fig. 5 are qualitatively understood as being due to reflection off a real barrier in the presence of a small amount of absorption. Because of the absorption, the turning point for the critical partial waves is pushed outwards [cf. eq. (3.6)]

to a position in qualitative agreement with what would be inferred from the Blair quarter point recipe based on a Coulomb trajectory†.

To assess the importance of the discrepancies between the WKB and exact phase shifts we compare the corresponding elastic cross sections in fig. 6. They were calculated utilizing the scattering amplitude

$$f(\theta) = f_{\mathrm{R}}(\theta) + \frac{i}{2k}\sum_{l}(2l+1)\mathrm{e}^{\mathrm{i}2\sigma_l}(1-\eta_l)P_l(\cos\theta), \tag{4.6}$$

where f_{R} is the Rutherford amplitude. The summation was carried out directly without using the saddle-point technique of refs. [3, 7]). The argreement in fig. 6 can be followed by another order of magnitude down before significant differences appear.

4 3 INELASTIC SCATTERING

We turn next to two examples of inelastic scattering. The first is a typical case of Coulomb-nuclear interference in the excitation of a low-lying collective state which will facilitate comparisons with previous semiclassical approaches. The second is an hypothetical nuclear excitation of a high-lying state for which previous approaches would break down.

We consider first the reaction ^{58}Ni(^{18}O, ^{18}O′)^{58}Ni(2^+; 1.45 MeV) at 60 MeV which was analyzed in DWBA using the optical parameters of table 1 and the collective form factor [10]) The analysis gives a satisfactory description of the data which shows the characteristic oscillations produced by Coulomb-nuclear interference [11]).

The WKB radial integrals for this case are given by (3 20). Part of the path of integration is shown in fig 4. Since the form factor is known as an analytic function on the real r-axis, we simply use it in the complex r-plane in connection with (3 20) Because this reaction is well matched there is no significant contribution coming from between the entrance and exit channel turning points. To check this we performed the integral of (3.20) clockwise as well as anticlockwise around the turning points and found no significant difference.

The radial integrals (3 20) were used to construct the total transition amplitude given by

$$T_{\beta\alpha}(\theta) = \sum_{l_\beta l_\alpha} i^{l_\alpha - l_\beta}(l_\beta\, m\lambda - m|l_\alpha 0)\sqrt{2l_\beta+1}\,\exp\left[i(\sigma_{l_\beta}+\delta_{l_\beta}+\sigma_{l_\alpha}+\delta_{l_\alpha})\right] I_{l_\beta l_\alpha}\, Y_{l_\beta m}(\theta, 0) \tag{4.7}$$

The corresponding angular distribution is shown in fig. 7 in comparison with the DWBA result. Note that in the WKB calculation we used the WKB nuclear phase shifts in (4.7).

In the present case the semiclassical expression for the matrix element obtained by inserting (3 23) into (3 20) can be used. The attempt in ref [4]) to use this approxi-

† Note that the derivative of the nuclear phase shifts with respect to l tends to zero for the critical partial waves so that the critical deflection angle becomes equal to the Rutherford value

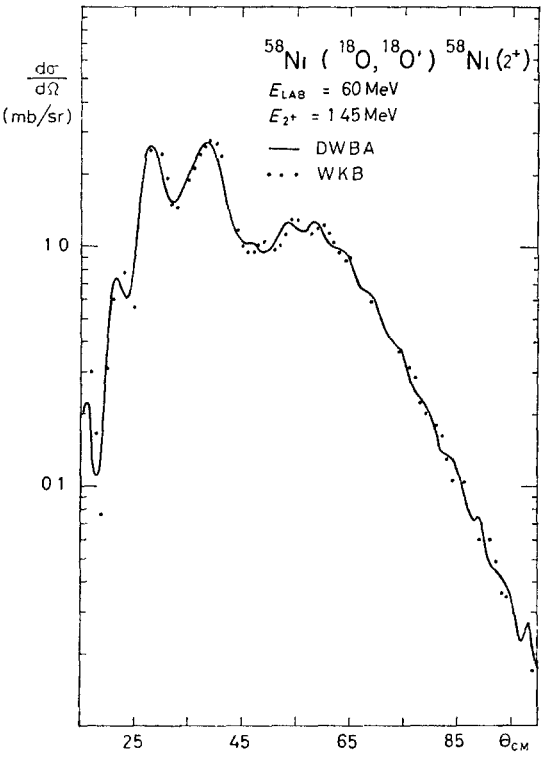

Fig. 7. Angular distribution for the inelastic scattering of ^{18}O with $E_{lab} = 60$ MeV exciting the first 2^+ state of ^{58}Ni The calculations use the optical parameters of table 1 and the collective nuclear form factor proportional to the derivative of the (complex) nuclear potential. Part of the path of integration for the WKB calculation using eq. (3.20) is shown in fig. 4. The entire path was rectangular extending out to 25 fm. Both calculations used partial waves up to $l_{max} = 100$ This accounts for the unphysical drop at forward angles and the small, high frequency oscillations appearing for $\theta_{c\,m} > 45°$. Both features are absent in the data analysis [10]) which used $l_{max} \approx 400$. The calculations shown actually fit the available data rather well

mation on a similar case failed because the wrong turning point was used when the barrier was exceeded [6]).

Two features make the previous case relatively simple from a semiclassical point of view. It is well matched and the long range quadrupole Coulomb interaction insures that Coulomb excitation contributes significantly, if not dominantly, to the final cross section. To check the range of validity of (3.20) we consider a hypothetical reaction ^{58}Ni(^{18}O, ^{18}O′)^{58}Ni(0^+; 10 MeV) again at 60 MeV in the entrance channel. We suppress the Coulomb excitation and use a form factor proportional to the derivative of the real nuclear potential The entrance and exit channel turning points given in fig. 8 show the large mismatch in the present case. Since the exit channel turning points are almost outside the range of the nuclear potential, the radial integrals receive large contributions from between the turning points.

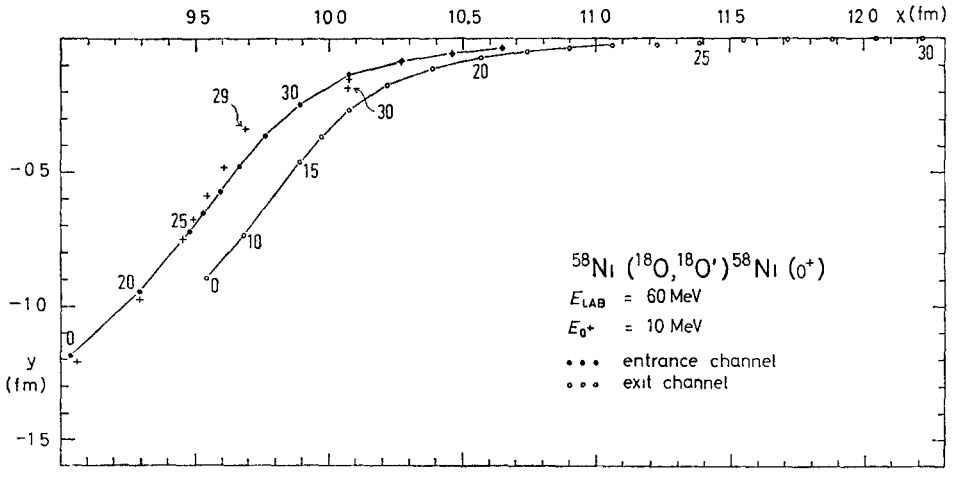

Fig. 8. Outermost turning points in the entrance channel (solid dots) and in the exit channel (open dots) for the fictitious reaction ^{58}Ni(^{18}O, ^{18}O')^{58}Ni(0^+; 10 MeV). The potential parameters are given in table 1. The plus signs result from taking the turning points of the real potential in the entrance channel and including the imaginary potential as a small perturbation according to eq (3.6).

The WKB and DWBA radial integrals for this case are compared in fig. 9. The largest deviation in the magnitude of the integrals occurs for partial wave $l = 18$ and is 8 %. In this example the correct sense of integration in (3.20) is clockwise. The results are an order of magnitude too large if the opposite sense is taken (cf. fig. 9)

Note that the radial integrals appear in the partial wave summation (4.7) multiplied by the average reflection coefficients

$$\eta_{l_\beta l_\alpha} = \exp\,[i(\delta_{l_\beta} + \delta_{l_\alpha})]. \tag{4.8}$$

In other words, the partial reaction amplitudes factorize into amplitudes for reflection depending only on the elastic scattering and transition amplitudes depending on the interaction coupling initial and final states. It is the decreasing amplitude for reflection as one goes above the Coulomb barrier which causes the reaction amplitudes to decrease for the low partial waves, giving rise to the familiar "surface peaking" in angular momentum space. The partial transition amplitudes, or radial integrals as we have defined them, increase rapidly as the turning points move into the range of nuclear interaction and then tend to saturate (see fig. 4).

In fig. 9 we also show the partial reaction amplitudes. The discrepancy with the DWBA for $l = 18$ increases to 13 % due to the inaccuracy of the WKB phase shifts This shows why the reaction cross sections are more sensitive to the elastic optical parameters than the elastic scattering itself [12]). The resulting WKB angular distribution is shown in fig. 10.

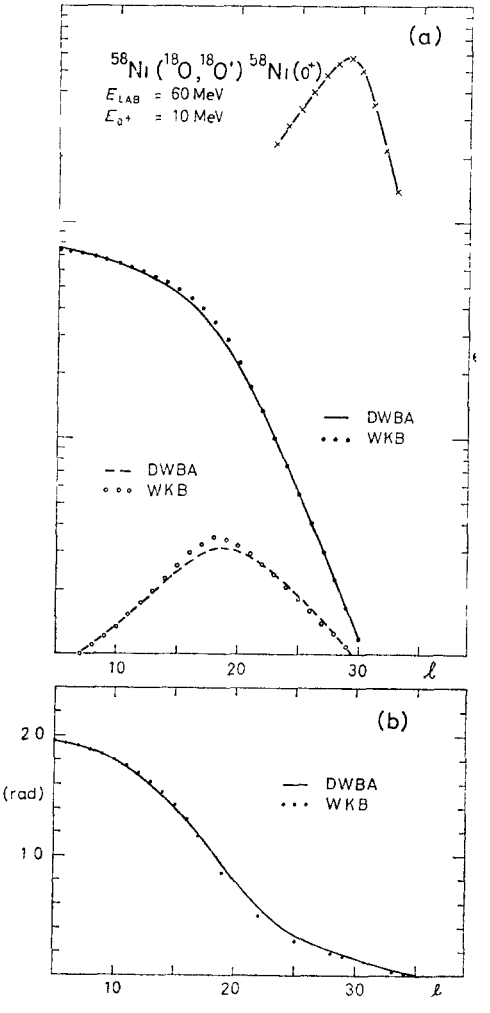

Fig. 9. Radial matrix elements for the fictitious reaction ^{58}Ni(^{18}O, ^{18}O')^{58}Ni(0$^+$; 10 MeV) at E_{lab} = 60 MeV The optical parameters in table 1 were used for the distorted waves while the form factor was taken to be proportional to the derivative of the real nuclear potential. Coulomb excitation is not included The solid dots in (a) are the magnitudes of the WKB integrals while a smooth solid line has been drawn through the corresponding DWBA results. In (b) the corresponding phases are plotted. The open circles and dashed lines in (a) result from multiplying the WKB and DWBA integrals by the corresponding average reflection coefficients The crossed line shows a few of the WKB integrals when the wrong sense of integration is used

4.4. ONE-PARTICLE TRANSFER

The above examples test the main approximation of using WKB wave functions with incoming wave boundary conditions. Previous semiclassical calculations of transfer reactions [13]) treated recoil approximately and were carried out along the real axis using a restricted class of optical potentials.

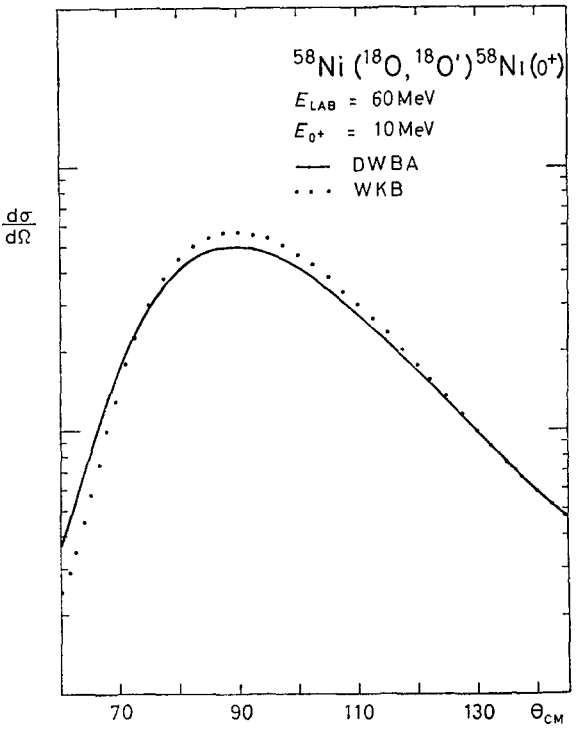

Fig. 10 Angular distribution for the reaction ^{58}Ni(^{18}O, ^{18}O′)^{58}Ni(0$^+$, 10 MeV) at E_{lab} = 60 MeV (cf fig 9) The units are arbitrary.

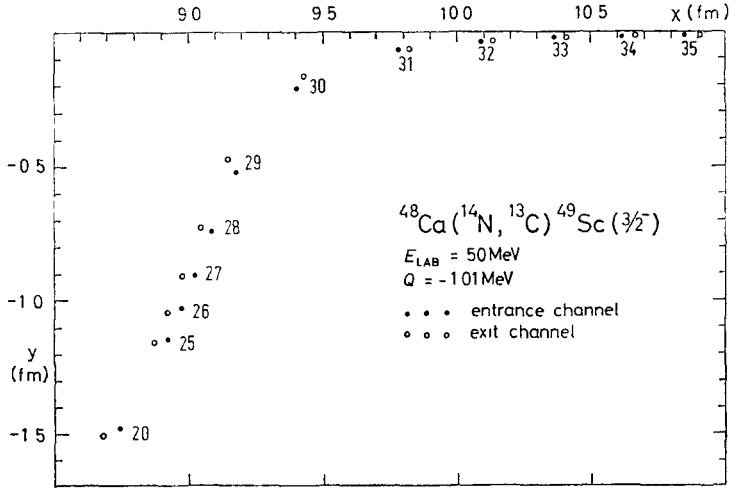

Fig. 11. Outermost turning points in the entrance and exit channels for the reaction ^{48}Ca(^{14}N, ^{13}C) ^{49}Sc($\frac{3}{2}^-$) at E_{lab} = 50 MeV using the optical potential given in table 1.

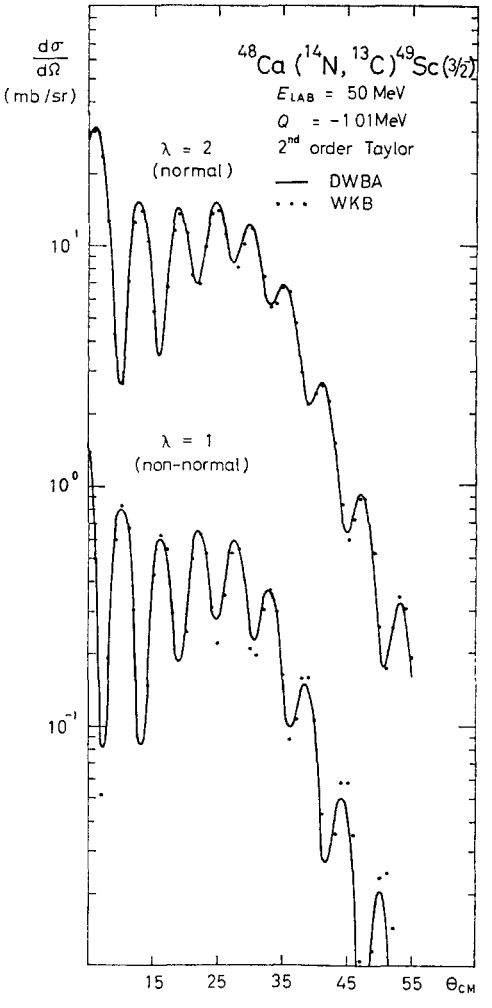

Fig 12 Angular distributions for the normal and non-normal angular momentum transfers in the reaction ^{48}Ca(^{14}N, ^{13}C)^{49}Sc($\frac{3}{2}^-$) at E_{lab} = 50 MeV.

We have studied the reaction ^{48}Ca(^{14}N, ^{13}C)^{49}Sc($\frac{3}{2}^-$; Q = −1.01 MeV) at 50 MeV. The optical parameters that were used are given in table 1. These parameters do not produce a quantitative fit to the corresponding data [14, 15]) but have been used to compare different DWBA computer codes which take recoil into account exactly†. The outermost turning points are shown in fig. 11. It is clear that this case is very well matched.

† We found that the imaginary potential was actually too weak to completely remove internal reflection. These features can be seen in the DWBA radial integrals but have little effect on the cross section

The form factors $f_{\lambda\mu'}(\nu, K^{\perp}, r_{\alpha})$ appearing in (3.21) were calculated numerically along the real axis for use in the DWBA calculation [16]). A pure $1p_{\frac{1}{2}}$ configuration wave function was used to describe the motion of the proton around ^{13}C while ^{49}Sc was described as a $2p_{\frac{1}{2}}$ proton moving around ^{48}Ca. We then parametrized these form factors by functions of the type

$$f_{\lambda\mu'}(\nu, K^{\perp}, r_{\alpha}) = Ae^{-\kappa r_{\alpha}}/r_{\alpha} \tag{4.9}$$

adjusting the values of A and κ by fitting the computed form factor at $r = 9$ fm and $r = 10$ fm. For the grazing partial waves the deviations from the true form factor at $r = 8$ fm and $r = 11$ fm were typically 5 % and 1 % respectively.

The comparison of DWBA and WKB cross sections is shown in fig 12 for both the normal and the non-normal angular momentum transfer. In this case we use the exact reflection coefficients (4 8) in the WKB calculation. When the WKB reflection coefficients are used the results are shifted to lie approximately 25 % above the DWBA curves.

The calculations shown in fig. 12 have been carried out to second order in the Taylor series, that is $\nu_{\max} = 2$ was used in (2.19) and (3.21). We have also compared the DWBA and WKB for $\nu_{\max} = 0$ and the agreement is equally good. The effect of the Taylor expansion is not very large in the present case. The zeroth-order results lie about 25 % below the second-order curves. However, the numerical calculations clearly show that the effect of the Taylor expansion of the wave function in (2 19) is accurately reproduced by the power series in the local momentum in (3.21).

5. Coupled equations

In this section we would like to point out that the WKB approach can readily be extended to coupled-channel problems. This is easiest to show if we neglect recoil and non-orthogonality effects since then the formalism of ref. [4]) may be taken over directly.

Thus we approximate the coupled-channel regular wave function in a particular channel β as

$$\tilde{\chi}_{\beta}(r) = c_{\beta}^{-}(r)\psi_{\beta}^{\text{in}}(r) + c_{\beta}^{+}(r)\psi_{\beta}^{\text{out}}(r), \tag{5.1}$$

where $\psi^{\text{out/in}}$ are the WKB approximations to the outgoing and ingoing solutions for the uncoupled problem as given by (3.9) and (3.10). Substituting (5.1) in the Schrödinger equation and neglecting second derivatives of $c^{\pm}$, linear equations for $c^{\pm}$ are obtained in the form

$$\frac{\mathrm{d}}{\mathrm{d}r} c_{\beta}^{\pm}(r) = \pm \sum_{\gamma} V_{\beta\gamma}(r)\psi_{\gamma}^{\text{out/in}}(r)\psi_{\beta}^{\text{in/out}}(r)c_{\gamma}^{\pm}(r). \tag{5.2}$$

The c^- amplitudes are integrated inwards starting with the boundary condition

$$c_\gamma^-(\infty) = \delta_{\gamma\alpha}, \tag{5.3}$$

α being the entrance channel. They are then matched to the c^+ amplitudes which in turn are integrated outwards The total scattering amplitude may be constructed from the asymptotic values of c^+ It is clear that outside the various turning points the outgoing set of equations is the analytic continuation of the ingoing set Thus the matching can be achieved by integrating the ingoing equations around the various turning points. The asymptotic values of c^+ are thus given by

$$c_\beta^+(\infty) = \delta_{\beta\alpha} - \int_C \mathrm{d}r \sum_\gamma \psi_\beta^{\mathrm{out}}(r) V_{\beta\gamma}(r) \psi_\gamma^{\mathrm{in}}(r) c_\gamma^-(r). \tag{5.4}$$

These equations have been applied below the Coulomb barrier to the problem of Coulomb excitation [17]) Substituting (5.3) into the right-hand side of (5.4) leads to eq. (3.20). Thus (5.4) is consistent with the first-order solution (3.20).

While it is clear from (5.2) that the integration path C must go around the various turning points, the manner in which this is to be done is not obvious. To study this problem we have considered the second-order solution to the quantum mechanical coupled-channel problem. Specializing to three channels α, β and γ corresponding to entrance, exit and intermediate channels respectively and assuming all diagonal matrix elements are zero, the second-order contribution to the reaction amplitude involves integrals of the type [18])

$$I_\beta = \int_0^\infty \mathrm{d}r\, \chi_\beta(r) V_{\beta\gamma}(r) \left[\chi_\gamma(r) \int_r^\infty \mathrm{d}r'\, h_\gamma^+(r') V_{\gamma\alpha}(r') \chi_\alpha(r') + h_\gamma^+(r) \int_0^r \mathrm{d}r'\, \chi_\gamma(r') V_{\gamma\alpha}(r') \chi_\alpha(r') \right], \tag{5.5}$$

where h^+ refers to the outgoing solutions of the uncoupled equations.

Assuming that the turning point r_0^β in the channel β lies to the left of turning point r_0^α, approximating χ by (3.7) and h^+ by

$$\tilde{h}^+(r) = \begin{cases} i\psi^{\mathrm{out}}(r), & \text{for } r > r_0 \\ \psi^{\mathrm{irreg}}(r), & \text{for } r < r_0, \end{cases} \tag{5.6}$$

the WKB expression for I_β may be evaluated for various locations of the turning point r_0^γ. Neglecting terms containing products of exponentially decreasing functions as was done in sect. 3 and utilizing the analytic properties summarized in fig 2 one finally arrives at the result

$$I_\beta = \tfrac{1}{8} i \int_C \mathrm{d}r\, \psi_\beta^{\mathrm{out}}(r) V_{\beta\gamma}(r) \psi_\gamma^{\mathrm{in}}(r) \int_{C(r)} \mathrm{d}r'\, \psi_\gamma^{\mathrm{out}}(r') V_{\gamma\alpha}(r') \psi_\alpha^{\mathrm{in}}(r'), \tag{5.7}$$

if r_0^γ lies between the turning points r_0^α and r_0^β. The path C goes anticlockwise around all three turning points. The label $C(r)$ means that the inner integration follows the same path as the outer integration up to the point r.

The sense of integration is the same as that required for the first order amplitudes The case when r_0^γ is between r_0^α and r_0^β is the most favored two step process from the point of view of Q-values. Therefore, we expect that use of the sense defined by the first-order transition may approximate higher order transitions as well.

6. Conclusions

The difficulties that were earlier encountered in using a semiclassical or a WKB treatment for heavy ion reactions above the Coulomb barrier have been solved by utilizing WKB solutions corresponding to an incoming wave boundary condition inside the barrier.

We have shown how to express the distorted wave matrix elements in terms of a loop integral around the complex turning points in the lower-half complex r-plane. This formulation provides a generalization of the classical orbital integral which can be also used for badly matched reactions where the Q-value is very different from its optimum value.

Through the systematic comparison of this method with DWBA calculations for reactions above the Coulomb barrier, we have shown how the cross sections are completely determined from the knowledge of the form factors and optical potentials in the neighborhood of the complex turning points close to the Coulomb barrier in the lower-half r-plane

The path integral concept is expected to provide a powerful technique also for coupled-channel calculations.

References

1) R A Broglia and Aa. Winther, Phys Reports **4C** (1972) 153
2) R. A Broglia, C H Dasso and Aa Winther, Phys. Lett. **53B** (1974) 301
3) J. Knoll and R. Schaeffer, Phys Lett. **52B** (1974) 131
4) R. A. Broglia, S. Landowne, R A. Malfliet, V. Rostokin and Aa. Winther, Phys Reports **11C** (1974) 1
5) R. A. Malfliet, Extended Seminar on nuclear physics ICTP, Trieste, Italy, Sept. 1973
6) T Koeling and R. A Malfliet, Phys. Reports **22C** (1975) 181
7) J Knoll and R Schaeffer, Preprint, Saclay DPh-T/75/40, April 1975
8) R A Broglia, R. Liotta, B S. Nilsson and Aa Winther, Phys. Reports, to be published
9) J. Heading, An introduction to phase-integral methods (Methuen, London, 1962)
10) F. Videbæk, P. R. Christensen, O. Hansen and K. Ulbak, Nucl. Phys. **A256** (1976) 301
11) P. R Christensen, I. Chernov, E E. Gross, R Stoksted and F. Videbæk, Nucl. Phys. **A207** (1973) 433
12) B. S Nilsson, R. A. Broglia, S. Landowne, R Liotta and Aa Winther, Phys Lett. **47B** (1973) 189
13) U Gotz, M. Ichimura, R. A. Broglia and Aa. Winther, Phys. Reports **16C** (1974) 116
14) M J Schneider, C. Chasman, E H. Auerbach, A. J. Baltz and S Kahana, Phys Rev Lett **31** (1973) 320
15) C Chasman, S Kahana and M J. Schneider, Phys Rev Lett **31** (1973) 1074
16) B. S Nilsson, unpublished
17) J. de Boer, H. Massman and Aa. Winther, Proc. Int. Workshop III on gross properties of nuclei, Hirschegg, Austria, 1975
18) K. Alder, F. Roesel and R. Morf, Nucl. Phys. **A186** (1972) 449